Matrix Biology Plus 21 (2024) 100141

Contents lists available at ScienceDirect

Matrix Biology Plus

journal homepage: www.sciencedirect.com/journal/matrix-biology-plus

Proteomic analysis of the extracellular matrix of human atherosclerotic plaques shows marked changes between plaque types

Lasse G. Lorentzen [a,1], Karin Yeung [b,c,1], Nikolaj Eldrup [b,c], Jonas P. Eiberg [b,c,d], Henrik H. Sillesen [b,c], Michael J. Davies [a,*]

[a] Department of Biomedical Sciences, Panum Institute, University of Copenhagen, Denmark
[b] Department of Vascular Surgery, Heart Centre, University Hospital Copenhagen - Rigshospitalet, Copenhagen, Denmark
[c] Department of Clinical Medicine, Faculty of Health and Medical Sciences, University of Copenhagen, Denmark
[d] Copenhagen Academy for Medical Education and Simulation (CAMES), Capital Region of Denmark, Copenhagen, Denmark

ARTICLE INFO

Keywords:
Atherosclerosis
Extracellular matrix
Proteomics
Carotid endarterectomy
Carotid artery stenosis

ABSTRACT

Cardiovascular disease is the leading cause of death, with atherosclerosis the major underlying cause. While often asymptomatic for decades, atherosclerotic plaque destabilization and rupture can arise suddenly and cause acute arterial occlusion or peripheral embolization resulting in myocardial infarction, stroke and lower limb ischaemia. As extracellular matrix (ECM) remodelling is associated with plaque instability, we hypothesized that the ECM composition would differ between plaques. We analyzed atherosclerotic plaques obtained from 21 patients who underwent carotid surgery following recent symptomatic carotid artery stenosis. Plaques were solubilized using a new efficient, single-step approach. Solubilized proteins were digested to peptides, and analyzed by liquid chromatography-mass spectrometry using data-independent acquisition. Identification and quantification of 4498 plaque proteins was achieved, including 354 ECM proteins, with unprecedented coverage and high reproducibility. Multidimensional scaling analysis and hierarchical clustering indicate two distinct clusters, which correlate with macroscopic plaque morphology (soft/unstable versus hard/stable), ultrasound classification (echolucent versus echogenic) and the presence of hemorrhage/ulceration. We identified 714 proteins with differential abundances between these groups. Soft/unstable plaques were enriched in proteins involved in inflammation, ECM remodelling, and protein degradation (e.g. matrix metalloproteinases, cathepsins). In contrast, hard/stable plaques contained higher levels of ECM structural proteins (e.g. collagens, versican, nidogens, biglycan, lumican, proteoglycan 4, mineralization proteins). These data indicate that a single-step proteomics method can provide unique mechanistic insights into ECM remodelling and inflammatory mechanisms within plaques that correlate with clinical parameters, and help rationalize plaque destabilization. These data also provide an approach towards identifying biomarkers for individualized risk profiling of atherosclerosis.

Introduction

Atherosclerotic plaques develop over many years and cause cardiovascular disease (CVD). While often asymptomatic for decades, atherosclerotic plaque destabilization and rupture can arise suddenly and cause acute thrombus or embolus in crucial organs. Extracellular matrix (ECM) remodelling can destabilize plaques, yet the mechanisms that give rise to unstable plaques are not fully understood. In this context, proteomic analyses of plaques, and their ECM composition have immense potential. However, such analyses remains a major challenge due to the dense network of cross-linked and fibrous proteins, which makes their extraction and subsequent data acquisition challenging. Thus, existing ECM proteomes are typically characterized by low protein numbers, low sequence coverage of detected species, and poor quantification. For these reasons, ECM proteomics remains a 'poor cousin' of cellular proteomics, and often results in an underestimation of the importance of the ECM in proteome studies.

As the numerical predominance of intracellular constituents in whole tissue lysates can interfere with the identification and quantification of both core- and ECM-associated (together termed 'the matrisome')

* Corresponding author.
E-mail address: davies@sund.ku.dk (M.J. Davies).
[1] Contributed equally to this work.

https://doi.org/10.1016/j.mbplus.2024.100141
Received 11 September 2023; Received in revised form 1 January 2024; Accepted 4 January 2024
Available online 11 January 2024

proteins by liquid chromatography-mass spectrometry (LC-MS), studies on the matrisome have often employed enrichment methods. These have typically used the low solubility of many ECM proteins to achieve this. In most cases, a mild buffer is used to lyse cells and remove soluble cellular material, leaving behind ECM materials. These are then analyzed via lengthy workflows with multiple extraction steps resulting in low sample throughput and material loss [1,2]. This results in dilemmas regarding analysis of all fractions, with adverse consequences for sample throughput, or only the ECM-enriched fractions. Examination of only the latter may result in material loss (e.g. due to solubility in lysis buffer), and bias regarding the number, quality and quantification of the proteins detected.

Recent developments in mass spectrometry (MS) instrumentation (e.g. trapped ion mobility spectrometers) and acquisition techniques (e.g. parallel accumulation-serial fragmentation combined with data-independent acquisition; DIA-PASEF), may mitigate some of the mentioned problems in matrisome proteomic studies. These new approaches potentially allow high proteome coverage within a single MS acquisition, avoiding complex sample processing and enrichment methods, loss of material and data, and the need to run samples under multiple different experimental conditions [3,4]. In light of these advances, this study employed a new simple, single-step protocol to extract proteins from human carotid artery atherosclerotic plaques, to determine in a proof-of-concept study if matrisome proteins differ between different plaque types and whether these correlate with macroscopic clinical examination (morphology, presence of hemorrhage, ulceration) and ultrasound images.

Histology has been widely used to categorize atherosclerotic plaques into stable and unstable types [5–8]. The stable plaques are typically characterized by extensive fibrosis and calcification which macroscopically is grossly expressed as 'hard' lesions. In contrast, unstable plaques usually have a soft consistency, and are considered rupture-prone due to high inflammatory activity. The unstable plaques have a thin fibrous cap, a large necrotic lipid core, and often intraplaque hemorrhage [5–8]. These characterizations are consistent with ultrasound echogenicity findings, with echogenic plaques expressing calcification and fibrosis being categorized as hard/stable, whereas echolucent plaques are assigned as unstable/soft [9–11]. However, plaques are highly heterogenous, particularly in advanced disease, and there is a need for a more reliable identification of unstable plaques and the drivers of instability. Such data could contribute to a more personalized risk stratification and patient-centric management of CVD, including an improved and more subtle selection of patients for carotid surgery, aggressive medical treatment, or a combination of both.

Currently, methods to assess plaque morphology in situ depend on imaging modalities, including ultrasound, computed tomography (CT) and magnetic resonance imaging (MRI). Regardless of the method, reliable and individual plaque morphology classification based on imaging is challenging, and not clinically implemented in symptomatic plaques and only to a limited extent in asymptomatic plaques [12]. Furthermore, such data have not been correlated with the ECM composition of plaques and proteomic data. This study aimed to determine: 1) whether a new single-step extraction procedure, combined with state-of-the-art LC-MS, would provide high-quality data on plaque proteomes and particularly the matrisome, without the need for prior enrichment or fractionation; 2) whether plaque types differentiate into specific clusters on the basis of their ECM protein composition; 3) whether such unbiased cluster analysis correlates with clinical assessment of the plaques into soft/rupture prone versus hard/stable on the basis of their macroscopic and ultrasonic characteristics; and 4) which biological pathways are modulated between cluster types.

Results

Coverage of the plaque proteome

Human symptomatic carotid atherosclerotic plaques (21 in total), obtained from patients who underwent carotid endarterectomy (for summary of patient data, see Supplementary Table 1), were analyzed using the protocol outlined in Fig. 1A. In total, 6839 proteins were identified at a 1 % false-discovery rate cut-off. After filtering out single peptide identifications and proteins with more than 10 missing values across all 21 samples, 4498 proteins were identified and quantified, including 354 matrisome proteins (137 core matrisome; 217 matrisome-associated) (Fig. 1B). The total proteome coverage, those categorized as cellular/plasma, total matrisome, and core matrisome / matrisome associated were all significantly greater than achieved in previous studies (Fig. 1B, C) [13–15], indicating that this single-step extraction procedure can provide high-quality and broad coverage of plaque proteomes and particularly the matrisome, without the need for prior enrichment or fractionation.

Quantitative analyses, as indicated by intensity-based absolute quantification (iBAQ) scores, show that core matrisome (Fig. 2A, green coloration) and matrisome-associated proteins (purple coloration) were among the most abundant proteins, when compared to the cellular and plasma division, in all plaques. The top 30 most abundant proteins from each division (cellular and plasma, matrisome, and matrisome associated) are presented in Figs. 2B–D respectively. Proteins are designated by gene names, with the rank numbers referring to their abundance (iBAQ score) in the total dataset. The number of peptides detected from each identified protein are also reported. The fractions of the total iBAQ intensity comprising cellular/plasma versus core matrisome and matrisome-associated species is presented in Fig. 2E, and that corresponding to different matrisomal sub-classes is presented in Fig. 2F.

Comparison of total proteome and matrisome data between plaques

Unsupervised clustering analysis was conducted using Monte-Carlo reference-based consensus clustering [16] to examine differences between the total proteomes of the atherosclerotic plaques, and whether these form well defined clusters depending on their protein composition. The Relative Cluster Stability Index reached a maximum at $k = 2$ (Fig. 3A), indicating a strong and consistent grouping of the data from the plaques into two clusters; a Monte Carlo p-value of < 0.05 at $k = 2$ supports this conclusion (Fig. 3B). Multidimensional scaling (MDS) analyses of the entire proteome dataset (Fig. 3C) and also the matrisome dataset (Fig. 3D) confirmed the presence of two distinct and well-separated clusters. Hierarchical clustering analysis, and the heatmap of the consensus index (Fig. 3E), confirmed the presence of two clusters based on the protein content of the plaques. These analyses strongly associate with independent (blinded) analysis of clinically-determined parameters including macroscopic morphology (soft/unstable, mixed, hard/stable; assessed visually), macroscopic presence of hemorrhage and plaque ulceration (both markers of potential plaque instability), as well as ultrasonic morphology (classification of the plaques on the basis of echolucent/echogenic image data) (Fig. 3E). Thus, the plaques classified macroscopically into soft and mixed were grouped, and strongly associated with Cluster 2, whereas those categorized as hard were strongly associated with Cluster 1.

Differences were detected in protein abundance between the two clusters, with 714 proteins of the total proteome dataset showing significant differential abundance using a false discovery rate (FDR) adjusted P value of < 0.05 (Fig. 4A). Among the proteins showing significant differential abundance, 59 were core matrisome proteins and 54 were ECM-associated proteins (Fig. 4B). The proteins (identified by gene names) with the largest fold changes in the total proteome dataset were examined for previous association with atherosclerosis through text

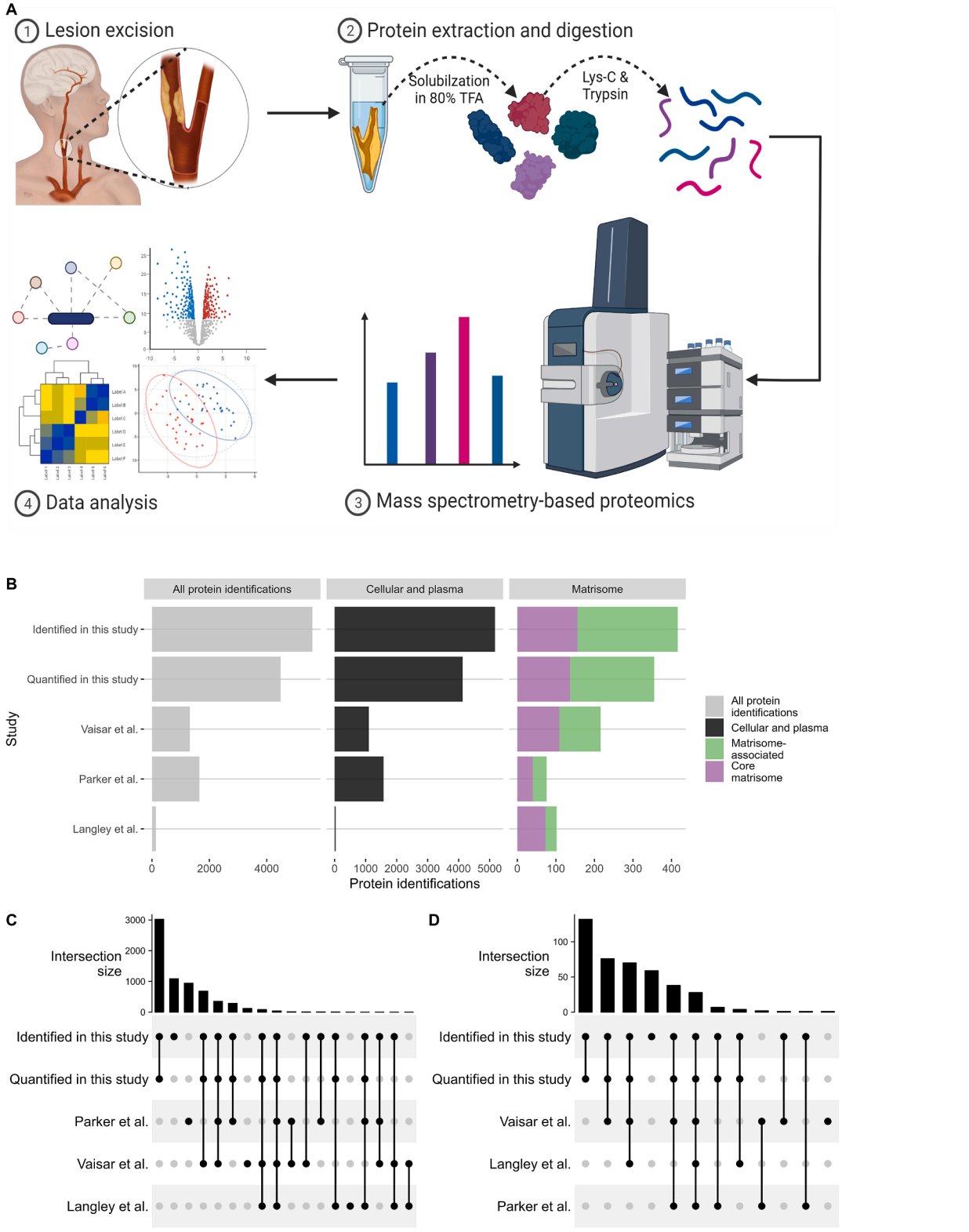

Fig. 1. Overview of the project workflow and liquid chromatography-mass spectrometry (proteomic) analysis. (A) Schematic overview of the experimental workflow. Plaques extracted during carotid endarterectomy were solubilized, cleaned-up, digested and analyzed by LC-MS as described in the Methods. (B) Bar plot showing the number of protein identifications and quantifications in this study and previous human plaque proteomics studies by Vaisar et al., Langley et al. and Parker et al. [13–15]. Plots present all protein identifications (grey bars), cellular and plasma proteins (black), and matrisome species, with the last of these further differentiated into core matrisome (purple) and matrisome-associated (green) proteins. (C) Upset plot showing the overlap of cellular and plasma protein identifications between this and previous studies. (D) As (C), except for matrisomal protein identifications. (For interpretation of the references to color in this figure legend, the reader is referred to the web version of this article.)

A

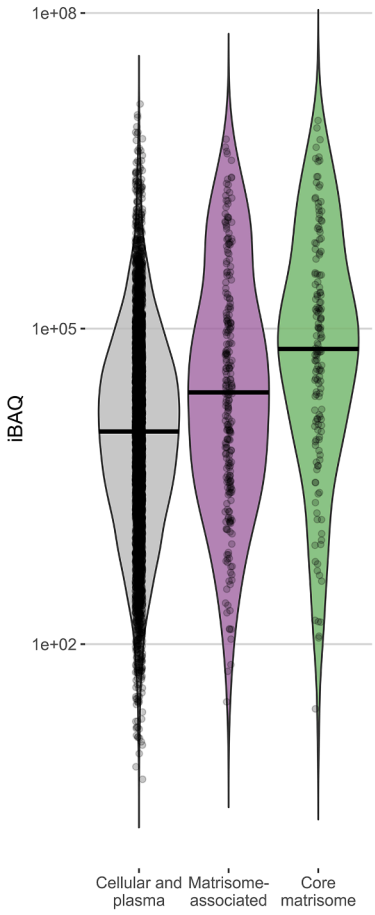

B

Rank	Gene	# Peptides
1	H4C1	9
2	ALB	79
3	APOA1	34
5	HBB	12
7	FTL	10
8	APCS	14
9	VIM	50
10	TAGLN	25
13	IGKC	8
16	IGHG2	8
17	AHSG	14
18	GAPDH	18
20	APOA2	9
22	TTR	10
27	HBA1	11
28	IGHG1	10
30	MYL9	11
31	IGHM	28
32	IGLC7	3
33	PFN1	14
35	APOE	33
36	APOA4	34
37	C3	119
38	CLU	24
39	SOD3	7
40	TF	61
41	C9	33
46	IGKV3-20	3
48	APOB	304
49	LYZ	9

C

Rank	Gene	# Peptides
11	S100A4	6
14	LGALS1	10
19	SERPINA1	33
21	ANXA2	35
25	S100A6	6
44	C1QB	8
45	SERPINC1	28
47	CTSD	23
56	A2M	80
58	HTRA1	26
69	SERPINA3	22
74	ANXA1	26
79	ANXA5	29
81	C1QC	7
84	S100A9	8
86	S100A8	10
92	F2	37
95	TGM2	29
107	SERPINF1	18
113	HPX	16
117	ANXA6	45
119	PLG	54
123	LGALS3	11
128	ITIH2	38
131	KNG1	24
132	SERPING1	23
137	CSTB	6
143	S100A11	5
149	CTSB	14
158	TIMP3	9

D

Rank	Gene	# Peptides
4	LUM	17
6	OGN	19
12	VTN	23
15	PRELP	20
23	FGG	36
24	FGB	41
26	BGN	20
29	FGA	49
42	MGP	6
43	EFEMP1	27
54	FN1	107
59	FMOD	11
63	COL6A3	170
80	SPP1	13
83	MFAP4	6
88	MFGE8	27
91	COL6A2	37
93	TGFBI	32
100	DPT	7
101	ASPN	20
108	FBLN5	14
120	POSTN	45
124	COL6A1	44
126	TNC	93
142	THBS1	51
147	COL14A1	67
150	COL1A2	29
157	COL1A1	33
165	IGFALS	22
174	AEBP1	36

E

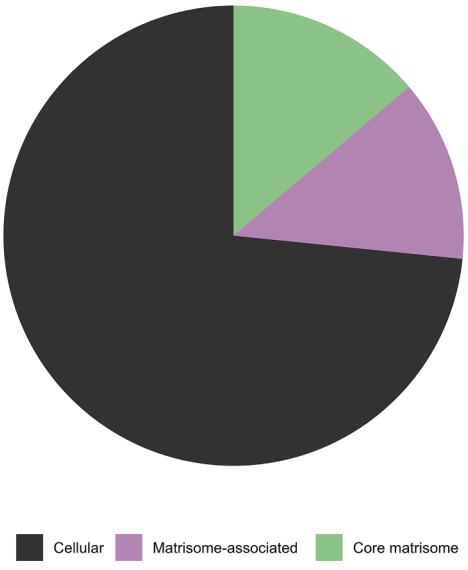

F

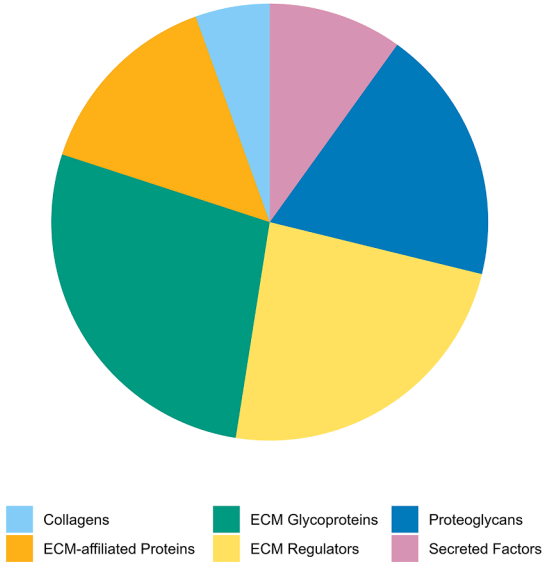

Fig. 2. Protein ranking by estimated absolute abundance. (A) Violin plots showing the distribution of intensity-based absolute quantification (iBAQ) values for cellular and plasma (grey), matrisome-associated (purple) and core matrisome (green) proteins, respectively. Crossbars indicate the median iBAQ values for each group. The full dataset is provided in Supplementary Table 2. (B - D) Identification and rank order of the 30 most abundant cellular and plasma (grey, panel B), matrisome-associated (purple, panel C) and core matrisome (green, panel D) proteins as designated by gene names. The number of identified peptides from each protein are also indicated. (D) The fraction of iBAQ intensity arising from cellular, core matrisome and matrisome-associated proteins. (E) The fraction of the total iBAQ intensity of proteins in each category (cellular/plasma, black; core matrisome, green; matrisome-associated, purple). (F) The fraction of iBAQ intensity within the matrisomal protein pool arising from collagens, proteoglycans, glycoproteins, matrisome regulators, matrix-affiliated proteins and secreted factors.

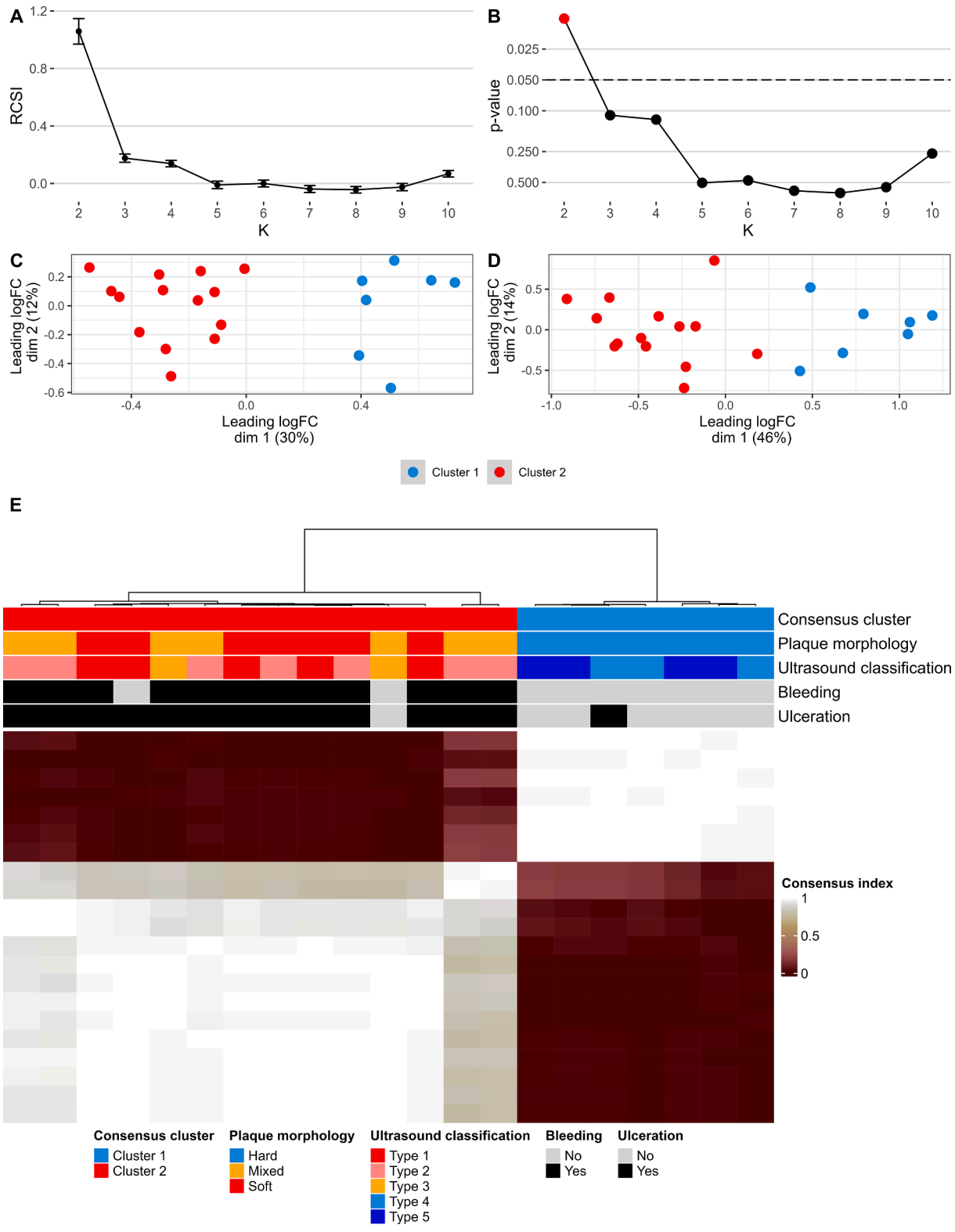

Fig. 3. Sample classification using consensus clustering of plaque proteome profiles. (A) Relative Cluster Stability Index for cluster numbers (k) 2–10 obtained by Monte Carlo reference-based consensus clustering. (B) P values for the distribution of stability scores being different from the null distribution at each k, indicating a statistically-significant preference for formation of two clusters. (C) Multidimensional scaling (MDS) plot of distances between protein abundance profiles for the total plaque proteome. Each sample is plotted on a two-dimensional scatterplot of the first two components of a MDS analysis for the top 500 most variable proteins, with each dot representing an individual plaque. Dots are color-coded according to their cluster assignment at k = 2. (D) As (C), but for the detected proteins present in the matrisome division of the plaque samples. (E) Cluster dendrogram and heatmap of consensus index (frequency of the sample pair being in the same cluster) for k = 2. Each sample is annotated with its assigned cluster, the macroscopic morphology of the plaque, the presence of plaque hemorrhage, ulceration of the endothelial layer, and classification of the plaque based on ultrasound imaging.

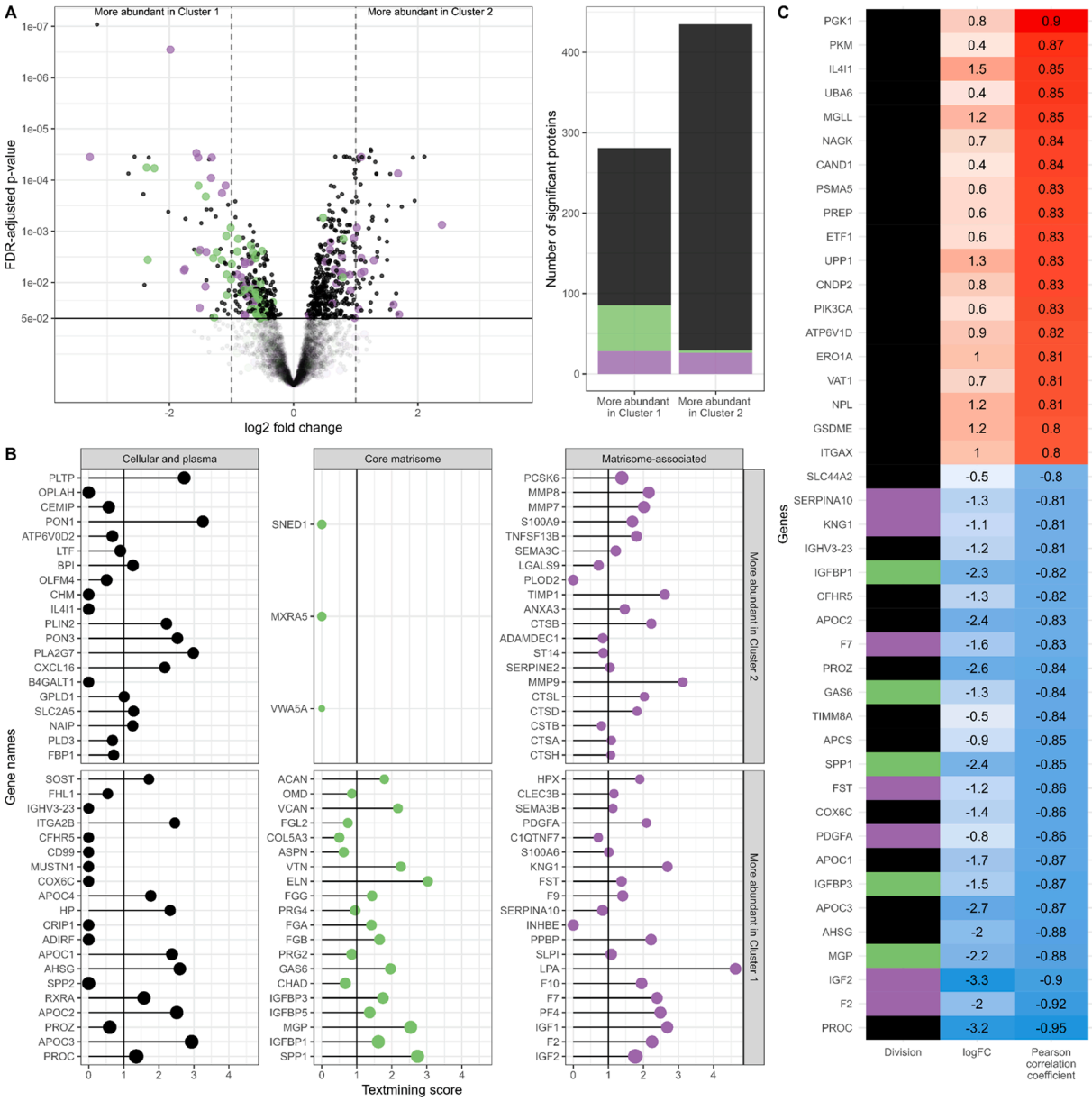

Fig. 4. Comparison of protein abundances between sample clusters. (A) Volcano plot of the total plaque proteome compared between Cluster 1 and Cluster 2 using robust linear modelling. Each point represents a protein with a log2 fold change between the samples compared (x axis), plotted against false discovery rate (FDR)–adjusted P (−log10 transformed, y axis). Black circles: cellular and plasma category; green circles: core matrisome; purple circles: matrisome associated. Gray circles indicate non-significant changes (adjusted P value > 0.05). The non-axial vertical lines denotes $\pm$ 1 fold change. (B) Lollipop plot of scores for association of total proteome dataset with atherosclerosis. According to the DISEASES database, the top 20 up- and downregulated proteins between Cluster 1 and Cluster 2 are shown with text mining scores for association with the term atherosclerosis. A score > 1 indicates substantial evidence for implication in atherosclerosis, where a lower score suggests few or no studies have reported previous links. A nonaxial vertical line at 1 indicates the median text mining score for all proteins in the database. Dot colors indicate the log2 fold change between Cluster 1 and Cluster 2 for each protein. (C) Tile plot showing Pearson correlation scores between protein label-free quantification (LFQ) intensities and plaque ultrasound classifications as well as log fold-change between Cluster 1 and Cluster 2. Only proteins with correlation score > 0.8 and FDR-adjusted p-value < 0.05 are shown. Black symbols: cellular and plasma proteins; purple symbols: matrisome-associated proteins; green symbols: core matrisome proteins. (For interpretation of the references to color in this figure legend, the reader is referred to the web version of this article.)

mining. Proteins that were more abundant in the plaques of Cluster 1 (categorized by gross morphology as 'hard') are presented in the upper part of Fig. 4C, whereas those that were more abundant in Cluster 2 (categorized macroscopically as 'soft/mixed') are presented in the lower part, with these color-coded to the protein division (as above). Correlations between the protein intensities (as determined by label-free quantification, LFQ) and log-fold change between Clusters 1 and 2, are presented in Fig. 4C, with the proteins categorized to their division by color coding.

Identification of pathways and processes that show differential regulation between the plaques in Cluster 1 versus Cluster 2

Processes and pathways associated with each cluster (i.e. those potentially associated with plaque stability / destabilization), were examined using gene ontology (GO) enrichment (Fig. 5A, B) and Reactome pathway analyses (Fig. 5C), with the fold changes between the plaque clusters used for ranking and scoring. These analyses indicate that multiple pathways related to ECM structure and organisation, ossification and mineralization, responses to wound healing, blood

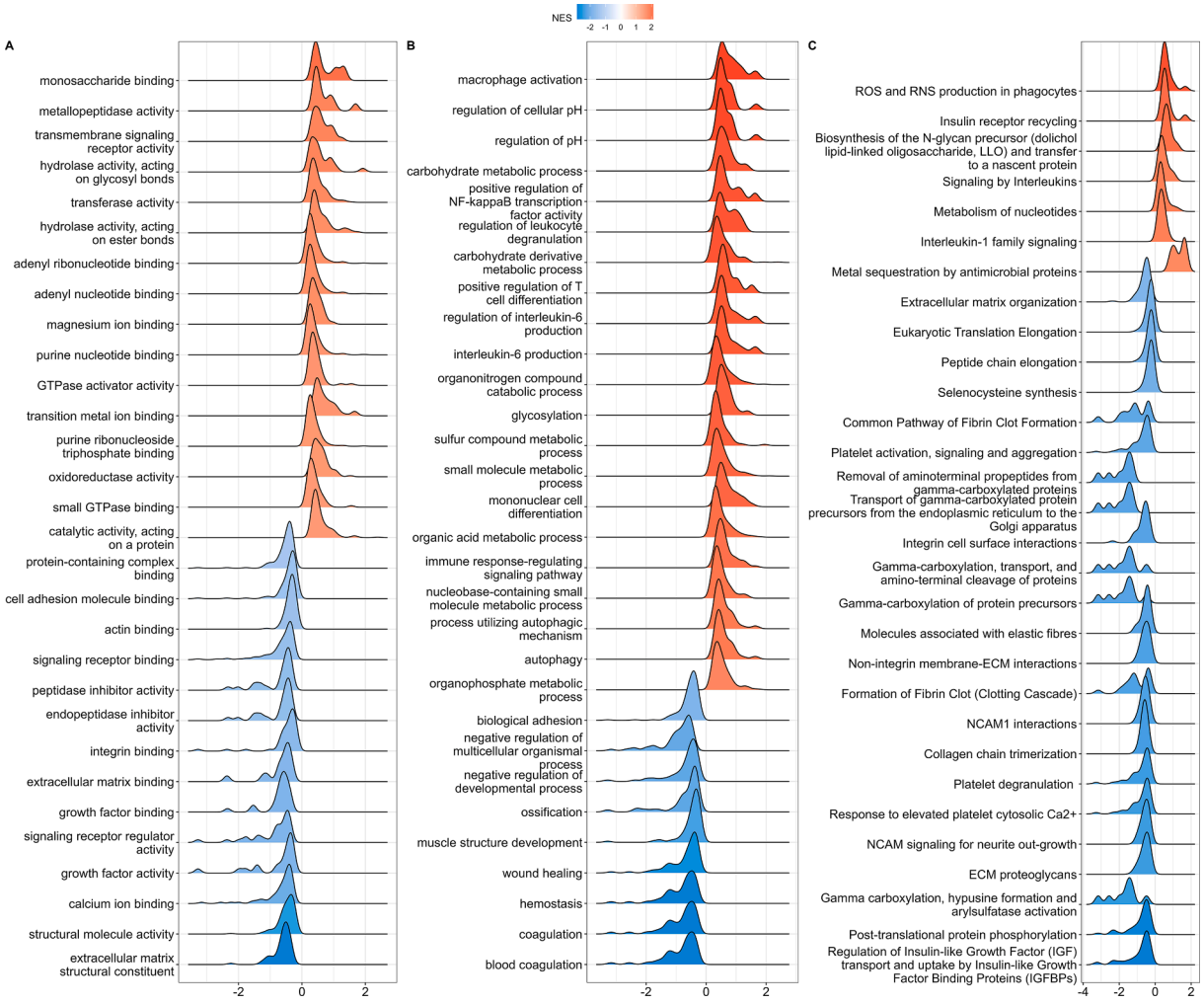

Fig. 5. Gene ontology (GO) and Reactome pathway enrichment analyses. Results from gene set enrichment analysis with log2 fold change between Cluster 1 (hard plaques) and Cluster 2 (soft and mixed) plaques using either gene ontology (GO) biological process (A) or molecular function terms (B), or Reactome pathways (C). The x-axis represents log2 fold change of genes in each term with the height of peaks indicating the density distribution. The density plots are colored by the normalized enrichment score (NES): positive values (colored red) represent up-regulation / enriched processes in Cluster 2, and negative values (colored blue) represent up-regulation / enriched processes in Cluster 1. (For interpretation of the references to color in this figure legend, the reader is referred to the web version of this article.)

clotting and platelet activation/degranulation were enriched in the plaques in Cluster 1 (categorized macroscopically as 'hard' plaques; Fig. 3E). In contrast, the plaques in Cluster 2 (categorized macroscopically as 'soft/mixed'; Fig. 3E) showed strong associations with inflammation (e.g. leukocyte activation, immune response pathways, cytokine production), reactive oxygen species/reactive nitrogen species (ROS/RNS) production and oxidoreductase activity, proteolytic activity (metallopeptidase and hydrolase activity and autophagy) and transition metal binding.

Protein-protein interaction network analysis

The Search Tool for the Retrieval of Interacting Genes/Proteins (STRING) tool was used to examine protein–protein interactions within the matrisome protein division. The resulting network is presented in Fig. 6. The nodes colored in red were detected as over-abundant in the plaques of Cluster 2 ('soft/mixed'), whereas those colored blue were over-abundant in Cluster 1 ('hard'). This analysis clearly indicates two strong and significant network clusters of over-abundant matrix metalloproteinases (MMPs 7, 8 and 9), together with a common inhibitor of these (TIMP1) enzymes, and cathepsins (A, B, D and L) in Cluster 2, with these (and particularly the MMPs) interacting with large numbers of core ECM structural proteins. Furthermore, multiple enzymes involved in collagen processing and modification (P4HA1, PLOD1 and 2) were also upregulated in Cluster 2 and show strong interactions with multiple collagen species as expected. In contrast, the plaques from Cluster 1 ('hard' plaques) showed significant upregulation and strong interactions between a very large number of ECM structural proteins, integrins and clotting proteins and coagulation factors.

Discussion

To succeed with personalized management of patients with CVD, new methods to distinguish the unstable plaque from stable, at an individual level, are needed. An increased understanding of the biochemical processes occurring within human atherosclerotic plaques may facilitate this [8,17].

The data reported here indicate that the fast, single-step, 'SPEED' extraction method is efficient in releasing both total proteins and ECM materials from human carotid artery plaques. The described approach allowed for a 70 % increase in detectable matrisome proteins compared to previous proteomic studies [13–15,18], and identified ~ 4500 proteins from human carotid plaques, including more than 350 matrisome proteins. Importantly, this method did not impair data breadth and

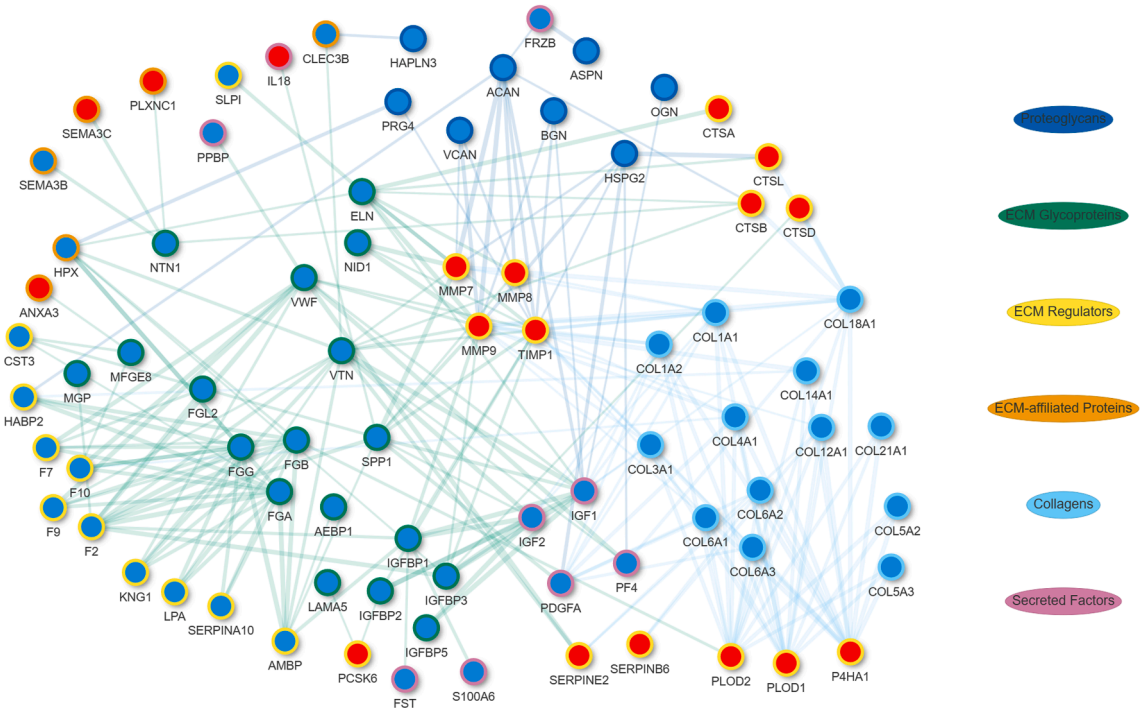

Fig. 6. Protein-protein interaction network of plaque matrisome proteins. Nodes are matrisome proteins that were detected as significantly different in their abundances (false discovery rate-adjusted p-value < 0.05) between Cluster 1 and Cluster 2. The central color of the nodes indicates if the proteins was observed as more abundant in Cluster 1 (blue nodes) or more abundant in Cluster 2 (red nodes). The colors of the node edges (outer rims of each circle) reflect the category of the matrisome proteins according to the matrisome database as indicated on the right side of the panel. Lines connecting nodes indicate interactions between core matrisome proteins and matrisome-associated proteins retrieved using The Search Tool for the Retrieval of Interacting Genes/Proteins (STRING) tool. Line widths indicate the confidence of interaction (only interactions with confidence > 0.4 are shown). Nodes with no interactions with confidence > 0.4 are omitted. (For interpretation of the references to color in this figure legend, the reader is referred to the web version of this article.)

quality, as only four previously-identified matrisome proteins were not detected when compared to literature data [13–15,18]. Division of the total pool into cellular/plasma, matrisome associated and core matrisome groups, showed that the matrisome, and particularly core matrisome proteins were highly abundant and over-represented in the total pool of proteins detected (Fig. 2A), though they were significantly less abundant in terms of the number of proteins identified (Fig. 2E). The matrisome division showed a wide spectrum of different classes of core and associated proteins (Fig. 2F). These data highlight the importance of the ECM and associated species in different types of plaques.

Cluster analysis of the total protein compositions of the plaques showed that these separated into two distinct, and significantly-different, groups (Fig. 3A, B). This separation was supported by multi-dimensional analyses carried out on both the total proteome (Fig. 3C), and those proteins ascribed to the matrisome division (Fig. 3D). This conclusion is supported by the unsupervised hierarchical clustering (Fig. 3E), with dramatic differences observed in the heat map between clusters 1 and 2. Of particular interest and importance, is the observation that this unbiased proteome analysis strongly matches the macroscopic clinical assessment of the plaques, with cluster 1 being assessed (independently from the proteome analysis) on the basis of gross morphology, as hard plaques, and cluster 2 as soft and mixed plaques. Similar associations were seen for the presence/absence of hemorrhage and ulceration, which were reported almost exclusively for the cluster 2 plaques. Classification of the ultrasound images into Types 1–5 also supported the clustering analysis, with all the plaques in cluster 2 being Type 1–3, signifying the presence of echolucent areas in the plaque imaging to a major (whole plaque; Type 1), or lesser extents (present but less that < 50 %; Type 3). Plaques in cluster 1 included ultrasound morphology Type 4 (more or less entirely echogenic) and interestingly also Type 5, which are interpreted as being heavily calcified over their entirety, although it is impossible to determine by ultrasound what lies behind acoustic shadowing. However, the proteomic data verify that the plaques classified by ultrasound as Types 4 and 5 are associated with an over-abundance of ECM structural proteins and those associated with calcification (see also below). The protein cluster analysis confirms the correlation between the gross macroscopic and ultrasound morphology, with the stable/unstable assumptions; hard plaques are echogenic on ultrasound implying greater plaque stability, while soft and mixed plaques showed considerable echolucent areas on ultrasound examination, indicating plaques with instability.

Over-representation analysis showed major differences in the abundance of 714 proteins between cluster 1 (hard/stable plaques) and cluster 2 (soft/unstable and mixed plaques), with a large number of the significant differences being core matrisome and matrisome-associated proteins (green and purple data points in Fig. 4A). These species also account for many of largest changes in abundance (i.e. those with the largest positive and negative log2 fold changes in Fig. 4A).

Detailed analysis indicates that cluster 1 (hard/stable plaques) have a higher level, and broader range of ECM materials. This may arise from increased ECM synthesis and deposition in these plaques, or alternatively increased ECM protein degradation via proteolytic or oxidative activity in cluster 2 (soft/unstable or mixed plaques). The data for matrisome proteins are summarized in Table 1; the full data set is presented in Supplementary Table 2. These data are consistent with previous studies on human carotid plaques [13,14]. Thus, Vaisar et al [13] reported that approximately 40 % of the proteins in ruptured plaques (soft plaques, categorized based on gross macroscopic evidence of ulceration and thrombus/hemorrhage) were altered in abundance. These include higher levels of proteins associated with proteolysis, inflammatory signalling, cell adhesion, cellular cytoskeleton and apoptosis, and decreased basement-membrane (ECM) proteins. Somewhat similar results have also been reported for carotid plaques by Langley et al [14]. However, less marked changes were detected in this earlier work for

Table 1
Summary of significant changes (adjusted p value < 0.05) in the abundance of matrisome proteins in 'soft' versus 'hard' plaques. Related proteins from the same family have been grouped in some cases.

Gene name	Protein name(s)	Known or potential function in artery wall
Overabundant in 'soft' plaques		
PLOD2, PLOD3	Procollagen-Lysine, 2-oxoglutarate 5-dioxygenases 2 and 3	Hydroxylation of Lys in collagen-like peptides used to generate ECM crosslinks. Activation of β-integrins.
VWA5A	Von Willebrand factor A domain-containing protein 5A	Unknown.
ADAMDEC1	A disintegrin and metalloproteinase like decysin	Matrix degradation.
PLXNC1	Plexin family	Transmembrane receptors for semaphorins. Potential regulation of cell migration, and immune response.
FCN3	Ficolin-3	Innate immunity through activation of the lectin complement pathway.
TIMP1	Tissue inhibitor of matrix metalloproteinases-1	Inhibition of tissue degradation by MMPs.
CTSB, CTSD, CTSH	Cathepsins-B, -D and -H	Cysteine (B,H) or Aspartate (D) proteases involved in protein turnover.
S100A9	S100 calcium-binding protein A9 / migration inhibitory factor-related protein 14 (MRP14) / calgranulin B. Forms calprotectin with S100A8	Calcium- and zinc-binding protein. Key role in the regulation of inflammatory processes and immune response.
MMP7, MMP9	Matrix metalloproteinases-7 and −9	Proteolysis of multiple ECM components.
ANXA3	Annexin A3	Regulation of cell growth and signal transduction. Inhibitor of phospholipase A2 and cleavage of inositol 1,2-cyclic phosphate. Role in anti-coagulation.
P4HA1	Prolyl 4-hydroxylase subunit alpha-1	Formation of 4-hydroxyproline and assembly of new collagen chains.
PCSK6	Proprotein Convertase Subtilisin / Kexin Type 6	Processing of protein precursors trafficking through secretory pathway.
CD109	Cluster of differentiation 109	Localises to surface of platelets, activated T-cells, and endothelial cells. Binds and negatively regulates TGF- β signaling.
SNED1	Sushi, Nidogen, and EGF-like Domains	Proposed to enable Notch binding activity and be involved in cell-matrix adhesion.
SEMA3C	Semaphorin 3C	Required for normal cardiovascular development. Binds to plexin family proteins.
MXRA5	Matrix-remodeling associated protein 5	Possible anti-inflammatory and anti-fibrotic properties. Limits cytokine induction, fibronectin and collagen expression in response to inflammatory stimuli.
TNFSF13B	Tumour necrosis factor superfamily member 13b	Stimulation of B- and T-cell function. Regulation of apoptosis.
ST14	Suppressor of tumourgenicity-14 / Matriptase	Serine protease.
Overabundant in 'hard' plaques		
MATN2	Matrilin 2	Formation of filamentous networks in ECM.
CHAD	Chondroadherin	Leucine-rich, matrix protein involved in cell adhesion.
MEGF6	Multiple epidermal growth factor-like Domains 6	Predicted to enable Ca^{2+} binding.
NTN1	Netrin-1	May direct retention of macrophages, promoting inflammation.
F2, F7, F9, F10	Prothrombin (F2), Coagulation factors 2, 7, 9, 10	Serine proteases involved in blood coagulation cascade.
KNG1	Kininogen-1 / α-2-thiol proteinase inhibitor	Inhibitor of cysteine proteases.
FGA	Fibrinogen alpha chain	Forms fibrin in blood clots.
PPBP	Pro-platelet basic protein	Platelet-derived growth of the CXC chemokine family.
PF4	Platelet factor 4	Cytokine of CXC chemokine family. Promotes blood clotting.
HPX	Hemopexin	Heme binding.
SLP1	Secretory leukocyte peptidase inhibitor-1	Inhibits trypsin, chymotrypsin, elastase, and cathepsin G.
VTN	Vitronectin	Binds to integrin αVβ3 promoting cell adhesion and spreading.
PDGFA	Platelet-derived growth factor subunit A	Regulates cell growth and division.
CLEC3B	C-Type Lectin Domain Family 3 Member B	Enables Ca^{2+}, heparin and kringle domain binding activity. Involved in mineralization.
S100A6, S100A10, S100A13, S100A16	Members of the S100 protein family	Regulate proliferation, apoptosis, cytoskeleton dynamics, and cell response to stress.
SOD3	Extracellular (Cu-Zn) superoxide dismutase-3	Conversion of superoxide radicals to hydrogen peroxide and oxygen.
MGP	Matrix Gla protein	Inhibitor of vascular mineralization.
LPA	Lipoprotein(a)	LDL variant. Risk factor for atherosclerosis.
SPP1	Osteopontin / bone sialoprotein I / early T-lymphocyte activation / secreted phosphoprotein 1	Integral part of mineralized ECM. Probably important for cell-ECM interactions.
VCAN	Versican	Large ECM proteoglycan with bound chondritin and keratan sulfate chains. Binds LDL.
NID1, NID2	Nidogens 1 and 2 (entactin)	Sulfated glycoproteins of basement membranes tightly associated with laminin. Binds collagen IV and perlecan. Role in cell-ECM interactions.
IGF2	Insulin-like growth factor 2	Growth-regulating, insulin-like and mitogenic activities. Binds to IGF-1 receptor.
IGFBP1, IGFBP2, IGFBP3, IGFBP5	Member of the insulin-like growth factor binding protein family	Prolong the half-life of IGFs and can inhibit or stimulate their growth-promoting effects.
FST	Follistatin	Binding and neutralisation of members of the TGF- β family.
OGN	Osteoglycin / mimecan	Small proteoglycan involved in mineralization.
COL1A2	Collagen-1, alpha-2 chain	Fibril-forming collagen.
COL5A1, COL5A2, COL5A3	Collagen-5, alpha-1, −2 and −3 chains	Fibrillar collagen.
COL6A1, COL6A2, COL6A3	Collagen-6, alpha-1, −2 and −3 chains	Beaded filament collagen involved in cell adhesion.
COL12A1	Collagen-12, alpha-1 chain	Fibril-associated collagen.
COL18A1	Collagen-18, alpha-1 chain	Multiplexin collagen.

(*continued on next page*)

Table 1 (*continued*)

Gene name	Protein name(s)	Known or potential function in artery wall
COL21A1	Collagen-21, alpha-1 chain	Collagen secreted by smooth muscle cells and may contribute to ECM assembly.
BGN	Biglycan	Small leucine-rich ECM proteoglycan. Involved in bone growth, muscle development/regeneration, and collagen fibril assembly. May regulate inflammation and innate immunity. Associated with atherosclerosis.
LUM	Lumican	Small leucine-rich ECM proteoglycan. Binds collagen fibrils and may regulate their growth.
PRELP	Proline And Arginine Rich End Leucine Rich Repeat Protein / Prolargin	Leucine-rich repeat ECM protein that functions to anchor basement membranes to connective tissue. Binds collagens-1 and −2.
MFAP4	Microfibril Associated Protein 4	ECM protein involved in cell adhesion and intercellular interactions.
INHBE	Inhibin subunit beta E	Member of the TGF- β superfamily. Regulates cell proliferation, apoptosis, immune response and hormone secretion.
TGFB2	Transforming growth factor beta 2 (TGF- β2)	Binds various TGF- β receptors. Recruits and activates SMAD family transcription factors and regulates gene expression.
DPT	Dermatopontin	ECM protein involved in cell-matrix interactions and matrix assembly. Proposed to modify TGF-β activity via interactions with decorin.
MFGE8	Milk Fat Globule EGF And Factor V/VIII Domain Containing	Preproprotein processed to multiple products, including lactadherin which promotes phagocytosis of apoptotic cells. Further processed to medin, the major protein of aortic medial amyloid.
SEMA3B	Semaphorin 3B	Class-3 semaphorin/ collapsin family member. May induce apoptosis.
FGL2	Fibrinogen Like 2	Protein similar to the beta- and gamma-chains of fibrinogen.
GAS6	Growth Arrest Specific 6	Gamma-carboxyglutamic acid (Gla)-containing protein proposed to be involved in stimulating cell proliferation. Associated with venous thromboembolic disease.
HABP2	Hyaluronan Binding Protein 2, Factor VII-Activating Protease	S1 family of serine proteases. Binds hyaluronic acid and involved in coagulation and fibrinolysis. Mutations associated with venous thromboembolism.
LTBP1, LTBP2, LTBP3, LTBP4	Latent Transforming Growth Factor Beta (TGF-b) Binding Proteins 1–4	Binds TGF-β, and targets complexes to the ECM.
C17orf58	Chromosome 17 Open Reading Frame 58	Part of collagen-containing ECM. Associated with posterior myocardial infarctions.
THSD4	Thrombospondin Type 1 Domain Containing 4	Predicted ECM structural constituent and involved in elastic fiber assembly.
PODN	Podocan	Small leucine-rich repeat protein. May function to inhibit smooth muscle cell proliferation and migration following arterial injury.
AEBP1	Adipocyte Enhancer Binding Protein 1	Carboxypeptidase A protein family member. May function as a transcriptional repressor and in smooth muscle cell differentiation.
ANGPTL6	Angiopoietin Like 6	Predicted to enable signalling receptor binding activity and be involved in angiogenesis and cell differentiation. Associated with collagen-containing ECM.
FRZB	Frizzled Related Protein	Modulator of Wnt signalling. Regulation of mineralization.
PRG4	Proteoglycan 4	Large proteoglycan with chondroitin sulfate and keratan sulfate.
OMD	Osteomodulin / Osteoadherin	Predicted to be involved in cell adhesion and regulation of mineralization.
C1QTNF3, C1QTNF7	C1q and TNF Related proteins 3 and 7	Predicted to be part of collagen trimers. Negative regulation of NIK/NF-κB signalling, and regulation of cytokine production.
ASPN	Asporin	Small leucine-rich proteoglycan family member. Binds collagen and Ca^{2+} and may induce mineralization.
TINAGL1	Tubulointerstitial Nephritis Antigen Like 1	Secreted glycoprotein. Induced by oxidised LDL.
SPON1	Spondin 1	Vascular smooth muscle cell growth-promoting factor. ECM structural component.
SERPINA10	Serpin Family A Member 10	Serine or cysteine proteinase inhibitor. Inhibits the activity of coagulation factors Xa and XIa. Mutations associated with venous thrombosis.

collagens [13], unlike the current study, where an over-abundance of multiple collagen isoforms was detected in hard plaques (COL1A2, COL5A1/A2/A3, COL6A1/A2/A3, COL12A1, COL18A1, COL21A1; Table 1). This could reflect more efficient protein extraction. Furthermore, multiple other core ECM proteins were also detected in this study as being over-abundant in hard plaques (MATN, FGA, FGL2, VCAN, NID1, NID2, BGN, LUM, MFAP4, DPT, HABP2, PODN, SPON1; Table 1) consistent with a greater extent of ECM synthesis and assembly. This is probably due to the higher numbers of synthetic smooth muscle cells in hard (stable) plaques.

The current data are consistent with the limited previous literature [13,14] suggesting that the instability of soft plaques (cluster 2) arises (at least partly) from an enhanced rate and extent of ECM degradation. This is supported by the text mining data presented for the top 20 up- and down-regulated proteins in Fig. 4B, with many of the scores showing a strong positive association (score $>$ 1) for association with atherosclerosis. The current study shows (Table 1) a significant enrichment in multiple proteases in cluster 2 plaques including MMPs-7, -8 and -9; matriptase (ST14), cathepsins-B (CTSB), -D (CTSD) and -H (CTSH), and a disintegrin and metalloproteinase like decysin (ADAMDEC1), together with tissue inhibitor of matrix metalloproteinases (TIMP1). Elevated levels of these proteins are consistent with enhanced ECM fragmentation and degradation.

Gene ontology (Fig. 5A, B) and Reactome analysis (Fig. 5C) further

support a role for proteolysis and oxidant generation in cluster 2 plaques, with the term 'ROS and RNS production in phagocytes' being the top Reactome pathway enrichment term (red density plots). Enhanced protease activity in cluster 2 (soft/unstable plaques) may be driven by, and synergistic with, oxidation-induced alterations, as a major phagocyte- (neutrophil/monocyte) derived protein, myeloperoxidase and its oxidation product, hypochlorous acid (HOCl) are able to convert inactive pro-MMPs to their active forms. This has been demonstrated in vitro for MMP-7 [19], MMP-8 [20] and MMP-9 [21,22]. In addition, ECM modification by oxidants, including HOCl and peroxynitrous acid/peroxynitrite, can modulate the expression and release of MMPs and ADAMTs, by both smooth muscle [23,24] and endothelial cells [25], and products consistent with such reactions have been detected in human arteriae femuralis and aortae abdominalis plaques [25–29]. In contrast, cluster 1 ('hard/stable') plaques showed (blue density plots) multiple terms and pathways associated with matrix synthesis and maintenance, as well as coagulation pathways, wound healing, calcium binding (calcification), cell adherence and binding and growth factor production.

Langley et al [14] have reported that symptomatic carotid plaques have a 'signature' that includes MMP-9, chitinase 3-like-1, S100 calcium-binding proteins A8 and A9 (S100A8 and S100A9), cathepsin B, fibronectin and galectin-3-binding protein. Several of these proteins (MMP-9, S100A9, cathepsin B), but not all, were detected as over-represented in the cluster 2 (soft/unstable) plaques in the current study. Some of these, and particularly MMP-9, have been reported to be involved in [30,31], and predictive of, major adverse clinical events (e.g. stroke and fatal cardiovascular disease [32,33]). The presence of both proteases and pro-inflammatory/oxidant-generating proteins that are released from activated neutrophils, and which stimulate phagocyte migration and activate endothelial cells (via Toll-like receptor 4 signalling), strongly support the hypothesis that high levels of ongoing inflammation and proteolysis contribute to enhanced ECM turnover in soft and mixed plaques.

Interestingly, high levels of 9 subunits of the V-type ATPase complex (ATP6V*) and carbonic anhydrase 12 (CA12) were observed in 'soft' plaques (Supplementary Table 2). The latter is a membrane-associated enzyme of the carbonic anhydrase family, reported to be expressed in colon, pancreas, kidney (including some carcinomas), prostate, ovary, testis, salivary gland and activated lymphocytes, but not erythrocytes, and therefore does not appear to arise from intra-plaque hemorrhage. The V-type ATPase family can activate proteases, and both enzyme families can demineralize the ECM through extracellular release of H^+ and Cl^-, and are associated with osteoclast-like cell activity. In ApoE knockout mice [34] both V-ATPase subunits, and multiple proteins associated with calcification including osteoactivin (GPNMB in humans), osteopontin (SPP1), bone sialoprotein 2 (IBSP), matrix Gla protein (MGP) and proteoglycan 4 (PRG4), were strongly increased in mature plaques containing large numbers of macrophages. A number of these proteins were also detected in the current study (SPP1, MGP, PRG4) in 'hard' plaques, together with other proteins associated with mineralization (osteoglycin/mimecan, OGN; osteomodulin, OMD; asporin, ASPN; the cellular protein alpha-2-Heremans-Schmid glycoprotein/fetuin A, AHSG) and signaling pathways associated with such processes (insulin-like growth factor-2, IGF2; and corresponding binding proteins, IGFBPs). This suggests a high and active turnover of calcified structures, indicating that mineralization / demineralization is an active process in advanced human carotid plaques. Previous studies have reported that 'spotty' (micro) calcification is associated with plaque rupture whereas extensive calcification is inversely correlated with rupture (reviewed [35]). Thus the crude description of plaques as 'hard' is a misleading and oversimplistic description (see also below). Whether microcalcification is associated with overexpression of the above proteins in specific regions of a plaque remains to be established, and indicates the need for spatially-resolved proteomic studies. It is also possible that extensively calcified regions of plaques may become less highly calcified, and more susceptible to rupture, as a result of demineralization processes as a result of overexpression of proteins that limit or reverse calcium deposition (e.g. ASPN, AHSG), or remove ECM species (e.g. specific glycosaminoglycans and proteoglycans) that act as calcification scaffolds. On the other hand, the surgeon's gross macroscopic "on-the-table" categorization into hard and soft plaque and its association with ultrasound and protein plaque analyses strengthens our findings' clinical perspective.

IGFBP1 and 5 are known to regulate smooth muscle cell migration and proliferation, cellular responses to cAMP, and are associated with fibrosis. GAS6 is also associated with cell growth and survival (including of endothelial cells), prevention of apoptosis, cell adhesion and cell migration. Several other highly-regulated matrisome proteins that have not been implicated previously in the pathophysiology of atherosclerosis have also been identified.

A major strength of this study is that it shows that proteomic identification and quantification of the proteins present in plaques correlates strongly with empirical clinical macroscopic assessment of plaque types. The unbiased cluster analyses of the protein complements of the plaques mirrors almost exactly with the plaque classification assessed by gross morphology, presence of hemorrhage or ulceration, and ultrasound analyses. Thus, the biochemistry of the plaques closely matches the clinical assessment of plaque type.

A further significant strength of this study is that we have developed and tested a workflow that allows efficient proteomic analysis of atherosclerotic plaques, with excellent coverage of intracellular and matrisome proteins. This method avoids the need for enrichment or fractionation steps and allows greater sample throughput. It also simplifies protein quantification since all precursor signals are present within a single MS acquisition. As both the extraction and clean-up are straightforward, analysis of larger sample numbers is practical and should allow better analysis of plaque variations, including those arising from age, sex, ethnicity and comorbidities. The relatively modest number of samples examined here (21), and the consequent lack of statistical power to examine these factors is a weakness, though sufficient to provide a clear proof-of-concept. Further weaknesses are a lack of data from asymptomatic plaques (as only symptomatic patients are operated in Denmark), data from earlier stages of atherosclerosis (which could not be obtained for ethical reasons), the weaknesses that subjective categorization ('hard', 'mixed' and 'soft') introduces, and an absence of complementary histology data, as the requirements for this are inconsistent with the proteomic processing employed.

The analysis of plaques in their entirety also carries certain drawbacks and limitations, as does the over-simplistic categorization of the plaques as 'soft', 'mixed' and 'hard'. Carotid plaques are heterogenous with different degrees of arteriosclerotic changes, calcification and multiple cell types. Proteome changes in the plaque shoulder regions may be particularly important for stability, disease severity and development [36]. This may be of particular relevance for mixed and ultrasound Type 3 plaques, in which soft and echolucent areas could respectively be identified but involve <50 % of the total plaque. Spatial assessment of the proteome within the plaque is not possible with the current approach, but recent technological advances have made it possible to link protein abundance to cellular phenotypes while preserving their spatial context [37].

Protein abundances from the current proteomics dataset clearly cluster into two groups as determined by multiple methods including cluster stability analysis via a Monte Carlo consensus approach, multidimensional scaling and hierarchical heatmaps. Around half of the proteins have been associated (to at least some extent) with atherosclerosis before, but a large number have no published association. This highlights a significant knowledge gap and further strengthens the need for new methods. These new identifications may be novel targets for therapeutic strategies aimed at unstable plaques. Additional work is required to clarify the role of these proteins and whether they can be manipulated therapeutically to minimize cardiovascular disease risk.

We and others have shown that proteomic analyses can provide unbiased and detailed biochemical data, but samples obtained through surgery have limited use in clinical assessment and patient management. In a recent proof-of-principal study, we showed that plaque proteins were retained on angioplasty balloons used during percutaneous intervention (PCI), and that this material could distinguish stable and unstable disease [38]. We speculate that a similar approach may be applicable to assess the stability of carotid atherosclerotic plaques without invasive surgery. Furthermore, proteins related to instability might be detected non-invasively e.g. by advanced ultrasound imaging. In such cases, plaques at high risk of causing future thrombotic events might be identified, and invasive or more aggressive treatment applied selectively for such cases.

While investigation of circulating tissue-derived biomarkers was outside the scope of the current study, others have used tissue data to guide the detection of plaque-derived materials in plasma [13–15]. Parker et al. used targeted MS-acquisition to identify species in the circulation that might disclose arterial disease [15]. However, this previous study did not address plaque instability, and it is unknown if and how such markers reflect the risk of complications. In another study, plaque stability was addressed by comparing symptomatic and asymptomatic carotid plaques [14], but these were not sub-grouped or stratified according to morphology. Proteomic and transcriptomic analyses identified four candidate markers that accurately reflected advanced atherosclerosis as measured by ultrasound, and improved risk prediction in two separate cohorts [14]. Interestingly, 3 of the 4 biomarkers (MMP9, CTSD and calprotectin) were also identified as being differentially expressed between soft and hard plaques in the current study. However, this previous study only identified 136 proteins in total, and only 30 proteins were differentially expressed between symptomatic and asymptomatic plaques at a modest (10 %) false discovery rate [14].

In conclusion, this study indicates that an efficient, single-step extraction procedure coupled with LC-MS/MS and data-independent acquisition allows unprecedented and reproducible identification and quantification of proteins from carotid plaques, including large numbers of previously unidentified species. Over 700 proteins have been identified with differential abundance between two clusters of plaques, that correlate with gross morphological and ultrasound analyses as hard (stable, cluster 1, echogenic) and soft (unstable, cluster 2, considerable echolucent areas) plaques. The second group (cluster 2) contains much lower levels of ECM proteins, and elevated levels of proteins involved in inflammation, oxidant formation and ECM remodelling. These data provide a unique insight into inflammatory mechanisms and ECM alterations as an explanation for plaque destabilization.

Experimental procedures

An expanded and detailed methods section is supplied in the Supplementary Data file.

Subjects and sample size

This study was designed as a proof-of-concept study, and thus we chose a sample size (7 hard, 7 soft, and 7 mixed, 21 in total) that would provide sufficient power to detect robust differences between the three plaque types in the presence of some technical variation.

Ethics

The study was conducted according to the Helsinki declaration, and data and biological materials were collected after patients' written, verbal, and informed consent. Study approval was obtained from The Danish National Committee on Health Research Ethics (journal number H-20002776).

Tissue samples

Carotid plaques from consecutive symptomatic patients, recently diagnosed with cerebral embolic ischaemia (stroke, transient ischaemic attack) or retinal ischaemia (complete vision loss, amaurosis fugax) were included. Patients were diagnosed, initially medically treated and subsequently referred for vascular surgery by departments of neurology. Internal carotid artery endarterectomy (surgery) for all patients was carried out at the same department of vascular surgery. Plaques were removed *in toto* using standard surgical techniques and then processed as described in the Supplementary Data. Immediately after the procedure, plaques were categorised as 'soft', 'hard' or 'mixed', based on gross macroscopic morphology by a consensus decision between the operating vascular surgeon and by the research-responsible vascular resident (KY, co-author). Besides overall consistency of plaque, details considered for categorization included calcification and fibrosis in 'hard' plaques and disintegrated content in 'soft' plaques, while mixed plaques had elements of both. In addition, the macroscopic presence of intraplaque hemorrhage (bleeding) and ulceration were noted by the operating surgeon, as such data are required documentation for standard patient care, and were not carried out specifically for this study. The macroscopic plaque categorization was determined before and independently of the proteomics analyses, with these carried out in a blinded manner.

Ultrasound analyses and classification

Extensive ultrasound imaging was performed on all carotid plaques by the research-responsible vascular resident (KY, co-author) 1–3 days before the operation. The imaging was recorded as short video clips (cine loops) in sweeping axial and longitudinal planes to capture the whole carotid plaque. Based on these ultrasound imaging cineloops, the plaques were categorized based on sonographic morphology using an established modified Gray-Weale classification as follows [40–42]; Type 1: $>$ 90 % uniformly echolucent (dark); Type 2: predominantly echolucent with $<$ 50 % echogenic areas; Type 3: predominantly echogenic plaque with $<$ 50 % echolucent areas, and Type 4: $>$ 90 % uniformly echogenic (bright). Type 5 plaques are those that could not be imaged properly by ultrasound due to shadowing, with this presumed to be due to heavy calcification [42]. The echogenic reference point was set as the vessel adventitia. Representative ultrasound images for all 5 types are shown in Supplementary Fig. 1.

Protein extraction, clean-up and digestion for proteomic analysis

Proteins were extracted from plaques using the Sample Preparation by Easy Extraction and Digestion (SPEED) protocol [43], and then cleaned up and digested as described by Batth et al [44] and in the Supplementary Data. Proteins were reduced and alkylated, digested using Lys-C and trypsin, then stored at − 80 °C until analysis. A schematic overview of the experimental workflow is presented in Fig. 1A.

Liquid chromatography-mass spectrometry (LC-MS/MS)

Samples were separated by LC and analyzed using a timsTOF mass spectrometer operated in a data-independent acquisition with parallel accumulation and serial fragmentation mode (DIA-PASEF; as described by Meier et al [4] and in the Supplementary Data).

Data analysis and statistical treatment

DIA-PASEF data were processed in DIA-NN [45,46] in library-free mode (see Supplementary Data). Peptides from digestion of the original proteins were identified by comparison with the UniProtKB protein database, including common contaminants. Intensity-based absolute quantification (IBAQ) values were calculated as described by Schwanhausser et al [47]. Further data analysis and visualisation were

performed as described in the Supplementary Data, with Benjamini–Hochberg adjusted p-values <0.05 considered significant [48,49].

The data in this report are either in the main text or Supplementary Data except for the raw MS files which have been deposited with the ProteomeXchange. This can be accessed as indicated in the text

All data are available within the article, in the Supplementary Data or, for mass spectrometry proteomics data, deposited to the ProteomeXchange Consortium via the PRIDE [39] partner repository with the dataset identifier PXD039077.

Author Contributions

L.G.L., N.E., J.E., H.S and M.J.D. conceived and designed the research. L.G.L., K.Y. and M.J.D. acquired the data and provided key resources for analysis. L.G.L. and K.Y. carried out statistical analysis. L.G.L., K.Y. and M.J.D. drafted the initial manuscript. L.G.L., K.Y., N.E., J.E., H.S and M.J.D. made critical revisions to the manuscript for intellectual content. L.G.L. and M.J.D. obtained funding. N.E., J.E., H.S and M.J.D. supervised and directed the study.

CRediT authorship contribution statement

Lasse G. Lorentzen: Writing – review & editing, Writing – original draft, Visualization, Methodology, Investigation, Funding acquisition, Formal analysis, Data curation, Conceptualization. **Karin Yeung:** . **Nikolaj Eldrup:** Writing – review & editing, Supervision, Conceptualization. **Jonas P. Eiberg:** Writing – review & editing, Supervision, Resources, Project administration, Formal analysis, Conceptualization. **Henrik H. Sillesen:** Writing – review & editing, Supervision, Project administration, Conceptualization. **Michael J. Davies:** Writing – review & editing, Writing – original draft, Supervision, Resources, Project administration, Funding acquisition, Formal analysis, Data curation, Conceptualization.

Declaration of competing interest

The authors declare that they have no known competing financial interests or personal relationships that could have appeared to influence the work reported in this paper.

Acknowledgements

This work was supported by grants from the Novo Nordisk Foundation (NNF13OC0004294 and NNF20SA0064214 to M.J.D.); and the Novo Nordisk Foundation-University of Copenhagen BRIDGE scheme (to L.G.L.).

Appendix A. Supplementary data

Supplementary data to this article can be found online at https://doi.org/10.1016/j.mbplus.2024.100141.

References

[1] M.C. McCabe, L.R. Schmitt, R.C. Hill, M. Dzieciatkowska, M. Maslanka, W. F. Daamen, T.H. van Kuppevelt, D.J. Hof, K.C. Hansen, Evaluation and refinement of sample preparation methods for extracellular matrix proteome coverage, Mol Cell Proteomics 20 (2021) 100079.
[2] S.J. Knott, K.A. Brown, H. Josyer, A. Carr, D. Inman, S. Jin, A. Friedl, S.M. Ponik, Y. Ge, Photocleavable surfactant-enabled extracellular matrix proteomics, Anal Chem 92 (24) (2020) 15693–15698.
[3] F. Meier, A.D. Brunner, S. Koch, H. Koch, M. Lubeck, M. Krause, N. Goedecke, J. Decker, T. Kosinski, M.A. Park, N. Bache, O. Hoerning, J. Cox, O. Rather, M. Mann, Online parallel accumulation-serial fragmentation (PASEF) with a novel trapped ion mobility mass spectrometer, Mol Cell Proteomics 17 (12) (2018) 2534–2545.
[4] F. Meier, A.D. Brunner, M. Frank, A. Ha, I. Bludau, E. Voytik, S. Kaspar-Schoenefeld, M. Lubeck, O. Raether, N. Bache, R. Aebersold, B.C. Collins, H.L. Rost, M. Mann, diaPASEF: parallel accumulation-serial fragmentation combined with data-independent acquisition, Nat Methods 17 (12) (2020) 1229–1236.
[5] A.C. Newby, Dual role of matrix metalloproteinases (matrixins) in intimal thickening and atherosclerotic plaque rupture, Physiol Rev 85 (1) (2005) 1–31.
[6] J.N. Redgrave, P. Gallagher, J.K. Lovett, P.M. Rothwell, Critical cap thickness and rupture in symptomatic carotid plaques: the oxford plaque study, Stroke 39 (6) (2008) 1722–1729.
[7] R. Virmani, A.P. Burke, A. Farb, F.D. Kolodgie, Pathology of the vulnerable plaque, J Am Coll Cardiol 47 (8 Suppl) (2006) C13–C18.
[8] G.K. Hansson, P. Libby, I. Tabas, Inflammation and plaque vulnerability, J Intern Med 278 (5) (2015) 483–493.
[9] M.L. Gronholdt, B.G. Nordestgaard, J. Bentzon, B.M. Wiebe, J. Zhou, E. Falk, H. Sillesen, Macrophages are associated with lipid-rich carotid artery plaques, echolucency on B-mode imaging, and elevated plasma lipid levels, J Vasc Surg 35 (1) (2002) 137–145.
[10] K. Skagen, K. Johnsrud, K. Evensen, H. Scott, K. Krohg-Sorensen, F. Reier-Nilsen, M.E. Revheim, J.G. Fjeld, M. Skjelland, D. Russell, Carotid plaque inflammation assessed with (18)F-FDG PET/CT is higher in symptomatic compared with asymptomatic patients, Int J Stroke 10 (5) (2015) 730–736.
[11] A.M. Johri, V. Nambi, T.Z. Naqvi, S.B. Feinstein, E.S.H. Kim, M.M. Park, H. Becher, H. Sillesen, Recommendations for the assessment of carotid arterial plaque by ultrasound for the characterization of atherosclerosis and evaluation of cardiovascular risk: from the american society of echocardiography, J Am Soc Echocardiogr 33 (8) (2020) 917–933.
[12] R. Naylor, B. Rantner, S. Ancetti, G.J. de Borst, M. De Carlo, A. Halliday, S. K. Kakkos, H.S. Markus, D.J.H. McCabe, H. Sillesen, J.C. van den Berg, M. Vega de Ceniga, M.A. Venermo, F.E.G. Vermassen, C. Esvs Guidelines, G.A. Antoniou, F. Bastos Goncalves, M. Bjorck, N. Chakfe, R. Coscas, N.V. Dias, F. Dick, R. J. Hinchliffe, P. Kolh, I.B. Koncar, J.S. Lindholt, B.M.E. Mees, T.A. Resch, S. Trimarchi, R. Tulamo, C.P. Twine, A. Wanhainen, R. Document, S. Bellmunt-Montoya, R. Bulbulia, R.C. Darling 3rd, H.H. Eckstein, A. Giannoukas, M.J. W. Koelemay, D. Lindstrom, M. Schermerhorn, D.H. Stone, Editor's choice - european society for vascular surgery (ESVS) 2023 clinical practice guidelines on the management of atherosclerotic carotid and vertebral artery disease, Eur J Vasc Endovasc Surg 65 (1) (2023) 7–111.
[13] T. Vaisar, J.H. Hu, N. Airhart, K. Fox, J. Heinecke, R.F. Nicosia, T. Kohler, Z. E. Potter, G.M. Simon, M.M. Dix, B.F. Cravatt, S.A. Gharib, D.A. Dichek, Parallel murine and human plaque proteomics reveals pathways of plaque rupture, Circ Res 127 (8) (2020) 997–1022.
[14] S.R. Langley, K. Willeit, A. Didangelos, L.P. Matic, P. Skroblin, J. Barallobre-Barreiro, M. Lengquist, G. Rungger, A. Kapustin, L. Kedenko, C. Molenaar, R. Lu, T. Barwari, G. Suna, X. Yin, B. Iglseder, B. Paulweber, P. Willeit, J. Shalhoub, G. Pasterkamp, A.H. Davies, C. Monaco, U. Hedin, C.M. Shanahan, J. Willeit, S. Kiechl, M. Mayr, Extracellular matrix proteomics identifies molecular signature of symptomatic carotid plaques, J Clin Invest 127 (4) (2017) 1546–1560.
[15] S.J. Parker, L. Chen, W. Spivia, G. Saylor, C. Mao, V. Venkatraman, R. J. Holewinski, M. Mastali, R. Pandey, G. Athas, G. Yu, Q. Fu, D. Troxlair, R. Vander Heide, D. Herrington, J.E. Van Eyk, Y. Wang, Identification of putative early atherosclerosis biomarkers by unsupervised deconvolution of heterogeneous vascular proteomes, J Proteome Res 19 (7) (2020) 2794–2806.
[16] C.R. John, D. Watson, D. Russ, K. Goldmann, M. Ehrenstein, C. Pitzalis, M. Lewis, M. Barnes, M3C: Monte Carlo reference-based consensus clustering, Sci Rep 10 (1) (2020) 1816.
[17] G.R. Geovanini, P. Libby, Atherosclerosis and inflammation: overview and updates, Clin Sci (lond) 132 (12) (2018) 1243–1252.
[18] M.H. Bao, R.Q. Zhang, X.S. Huang, J. Zhou, Z. Guo, B.F. Xu, R. Liu, Transcriptomic and proteomic profiling of human stable and unstable carotid atherosclerotic plaques, Front Genet 12 (2021) 755507.
[19] X. Fu, S.Y. Kassim, W.C. Parks, J.W. Heinecke, Hypochlorous acid oxygenates the cysteine switch domain of pro- matrilysin (MMP-7). A mechanism for matrix metalloproteinase activation and atherosclerotic plaque rupture by myeloperoxidase, J. Biol. Chem. 276 (2001) 41279–41287.
[20] J. Michaelis, M.C. Vissers, C.C. Winterbourn, Different effects of hypochlorous acid on human neutrophil metalloproteinases: activation of collagenase and inactivation of collagenase and gelatinase, Arch Biochem Biophys 292 (2) (1992) 555–562.
[21] G.J. Peppin, S.J. Weiss, Activation of the endogenous metalloproteinase, gelatinase, by triggered human neutrophils, Proc Natl Acad Sci U S A 83 (12) (1986) 4322–4326.
[22] Y. Wang, C.Y. Chuang, C.L. Hawkins, M.J. Davies, Activation and inhibition of human matrix metalloproteinase-9 (MMP9) by HOCl, myeloperoxidase and chloramines, Antioxidants (Basel) 11 (8) (2022).
[23] H. Cai, C.Y. Chuang, S. Vanichkitrungruang, C.L. Hawkins, M.J. Davies, Hypochlorous acid-modified extracellular matrix contributes to the behavioral switching of human coronary artery smooth muscle cells, Free Radic Biol Med 134 (2019) 516–526.
[24] S.M. Jorgensen, L.G. Lorentzen, C.Y. Chuang, M.J. Davies, Peroxynitrous acid-modified extracellular matrix alters gene and protein expression in human coronary artery smooth muscle cells and induces a pro-inflammatory phenotype, Free Radic Biol Med 186 (2022) 43–52.
[25] S. Vanichkitrungruang, C.Y. Chuang, C.L. Hawkins, A. Hammer, G. Hoefler, E. Malle, M.J. Davies, Oxidation of human plasma fibronectin by inflammatory oxidants perturbs endothelial cell function, Free Radic Biol Med 136 (2019) 118–134.
[26] J.S. Beckman, Y.Z. Ye, P.G. Anderson, J. Chen, M.A. Accavitti, M.M. Tarpey, C. R. White, Extensive nitration of protein tyrosines in human atherosclerosis

detected by immunohistochemistry, Biol. Chem. Hoppe-Seyler 375 (2) (1994) 81–88.
[27] E. Malle, G. Waeg, R. Schreiber, E.F. Grone, W. Sattler, H.J. Grone, Immunohistochemical evidence for the myeloperoxidase/H2O2/halide system in human atherosclerotic lesions: colocalization of myeloperoxidase and hypochlorite-modified proteins, Eur J Biochem / FEBS 267 (14) (2000) 4495–4503.
[28] C.Y. Chuang, G. Degendorfer, A. Hammer, J.M. Whitelock, E. Malle, M.J. Davies, Oxidation modifies the structure and function of the extracellular matrix generated by human coronary artery endothelial cells, Biochem J 459 (2014) 313–322.
[29] G. Degendorfer, C.Y. Chuang, H. Kawasaki, A. Hammer, E. Malle, F. Yamakura, M. J. Davies, Peroxynitrite-mediated oxidation of plasma fibronectin, Free Radic Biol Med 97 (2016) 602–615.
[30] J. Sun, P. Singh, A. Shami, E. Kluza, M. Pan, D. Djordjevic, N.B. Michaelsen, C. Kennback, N.N. van der Wel, M. Orho-Melander, J. Nilsson, I. Formentini, K. Conde-Knape, E. Lutgens, A. Edsfeldt, I. Goncalves, Spatial transcriptional mapping reveals site-specific pathways underlying human atherosclerotic plaque rupture, J Am Coll Cardiol 81 (23) (2023) 2213–2227.
[31] C. Giannarelli, Single-Point Vulnerabilities in Atherosclerotic Plaque, J Am Coll Cardiol 81 (23) (2023) 2228–2230.
[32] N. Eldrup, M.L. Gronholdt, H. Sillesen, B.G. Nordestgaard, Elevated matrix metalloproteinase-9 associated with stroke or cardiovascular death in patients with carotid stenosis, Circulation 114 (17) (2006) 1847–1854.
[33] S. Blankenberg, H.J. Rupprecht, O. Poirier, C. Bickel, M. Smieja, G. Hafner, J. Meyer, F. Cambien, L. Tiret, I. AtheroGene, Plasma concentrations and genetic variation of matrix metalloproteinase 9 and prognosis of patients with cardiovascular disease, Circulation 107 (12) (2003) 1579–1585.
[34] M. Wierer, M. Prestel, H.B. Schiller, G. Yan, C. Schaab, S. Azghandi, J. Werner, T. Kessler, R. Malik, M. Murgia, Z. Aherrahrou, H. Schunkert, M. Dichgans, M. Mann, Compartment-resolved Proteomic Analysis of Mouse Aorta during Atherosclerotic Plaque Formation Reveals Osteoclast-specific Protein Expression, Mol Cell Proteomics 17 (2) (2018) 321–334.
[35] X. Shi, J. Gao, Q. Lv, H. Cai, F. Wang, R. Ye, X. Liu, Calcification in atherosclerotic plaque vulnerability: friend or foe? Front Physiol 11 (2020) 56.
[36] J.F. Bentzon, F. Otsuka, R. Virmani, E. Falk, Mechanisms of plaque formation and rupture, Circ Res 114 (12) (2014) 1852–1866.
[37] A. Mund, F. Coscia, A. Kriston, R. Hollandi, F. Kovacs, A.D. Brunner, E. Migh, L. Schweizer, A. Santos, M. Bzorek, S. Naimy, L.M. Rahbek-Gjerdrum, B. Dyring-Andersen, J. Bulkescher, C. Lukas, M.A. Eckert, E. Lengyel, C. Gnann, E. Lundberg, P. Horvath, M. Mann, Deep visual proteomics defines single-cell identity and heterogeneity, Nat Biotechnol 40 (8) (2022) 1231–1240.
[38] L.G. Lorentzen, G.M. Hansen, K.K. Iversen, H. Bundgaard, M.J. Davies, Proteomic characterization of atherosclerotic lesions in situ using percutaneous coronary intervention angioplasty balloons, Arterioscler Thromb Vasc Biol 42 (7) (2022) 857–864.
[39] Y. Perez-Riverol, J. Bai, C. Bandla, D. Garcia-Seisdedos, S. Hewapathirana, S. Kamatchinathan, D.J. Kundu, A. Prakash, A. Frericks-Zipper, M. Eisenacher, M. Walzer, S. Wang, A. Brazma, J.A. Vizcaino, The PRIDE database resources in 2022: a hub for mass spectrometry-based proteomics evidences, Nucleic Acids Res 50 (D1) (2022) D543–D552.
[40] A.C. Gray-Weale, J.C. Graham, J.R. Burnett, K. Byrne, R.J. Lusby, Carotid artery atheroma: comparison of preoperative B-mode ultrasound appearance with carotid endarterectomy specimen pathology, J Cardiovasc Surg (torino) 29 (6) (1988) 676–681.
[41] L.M. Reilly, R.J. Lusby, L. Hughes, L.D. Ferrell, R.J. Stoney, W.K. Ehrenfeld, Carotid plaque histology using real-time ultrasonography, Clinical and Therapeutic Implications, Am J Surg 146 (2) (1983) 188–193.
[42] G. Geroulakos, G. Ramaswami, A. Nicolaides, K. James, N. Labropoulos, G. Belcaro, M. Holloway, Characterization of symptomatic and asymptomatic carotid plaques using high-resolution real-time ultrasonography, Br J Surg 80 (10) (1993) 1274–1277.
[43] J. Doellinger, A. Schneider, M. Hoeller, P. Lasch, Sample preparation by easy extraction and digestion (SPEED) - a universal, rapid, and detergent-free protocol for proteomics based on acid extraction, Mol Cell Proteomics 19 (1) (2020) 209–222.
[44] T.S. Batth, M.X. Tollenaere, P. Ruther, A. Gonzalez-Franquesa, B.S. Prabhakar, S. Bekker-Jensen, A.S. Deshmukh, J.V. Olsen, Protein aggregation capture on microparticles enables multipurpose proteomics sample preparation, Mol Cell Proteomics 18 (5) (2019) 1027–1035.
[45] V. Demichev, C.B. Messner, S.I. Vernardis, K.S. Lilley, M. Ralser, DIA-NN: neural networks and interference correction enable deep proteome coverage in high throughput, Nat Methods 17 (1) (2020) 41–44.
[46] V. Demichev, L. Szyrwiel, F. Yu, G.C. Teo, G. Rosenberger, A. Niewienda, D. Ludwig, J. Decker, S. Kaspar-Schoenefeld, K.S. Lilley, M. Mulleder, A. I. Nesvizhskii, M. Ralser, dia-PASEF data analysis using FragPipe and DIA-NN for deep proteomics of low sample amounts, Nat Commun 13 (1) (2022) 3944.
[47] B. Schwanhausser, D. Busse, N. Li, G. Dittmar, J. Schuchhardt, J. Wolf, W. Chen, M. Selbach, Global quantification of mammalian gene expression control, Nature 473 (7347) (2011) 337–342.
[48] Y. Benjamini, Y. Hochberg, Controlling the false discovery rate: A practical and powerful approach to multiple testing, J Roy Stat Soc Series B. 57 (1995) 289–300.
[49] A. Sticker, L. Goeminne, L. Martens, L. Clement, Robust Summarization and Inference in Proteome-wide Label-free Quantification, Mol Cell Proteomics 19 (7) (2020) 1209–1219.